Molecular Basis of Cell and Developmental Biology:

Elucidation, Quantitative Refinement, and *in Vivo* Utilization of the HOXA13 DNA Binding Site

Wendy M. Knosp, Chie Saneyoshi, Siming Shou, Hans Peter Bächinger and H. Scott Stadler

J. Biol. Chem. 2007, 282:6843-6853.
doi: 10.1074/jbc.M610775200 originally published online January 1, 2007

THE JOURNAL OF BIOLOGICAL CHEMISTRY VOL. 282, NO. 9, pp. 6843–6853, March 2, 2007

Elucidation, Quantitative Refinement, and *in Vivo* Utilization of the HOXA13 DNA Binding Site*[S]

Received for publication, November 21, 2006 Published, JBC Papers in Press, January 1, 2007, DOI 10.1074/jbc.M610775200

Wendy M. Knosp[‡§], **Chie Saneyoshi**[‡], **Siming Shou**[‡], **Hans Peter Bächinger**[¶‖], **and H. Scott Stadler**[‡‖1]

From the Departments of [‡]*Molecular and Medical Genetics and* [¶]*Biochemistry and Molecular Biology, Oregon Health and Science University, Portland, Oregon 97239, the* [§]*Department of Anatomy, University of California San Francisco, San Francisco, California 94158-2324, and the* [‖]*Research Division, Shriners Hospital for Children, Portland, Oregon 97239*

Mutations in *Hoxa13* cause malformations of the appendicular skeleton and genitourinary tract, including digit loss, syndactyly, and hypospadias. To determine the molecular basis for these defects, the DNA sequences bound by HOXA13 were empirically determined, revealing a novel high affinity binding site. Correlating the utilization of this high affinity binding site with genes exhibiting perturbed expression in *Hoxa13* mutant limbs, we identified that HOXA13 suppresses the expression of the BMP antagonist, *Sostdc1*. In the absence of HOXA13 function, *Sostdc1* is ectopically expressed in the distal limb, causing reduced expression of BMP-activated genes and decreased SMAD phosphorylation. Limb chromatin immunoprecipitation revealed HOXA13 binding at its high affinity site in two conserved *Sostdc1* regulatory sites *in vivo*. *In vitro*, HOXA13 represses gene expression through the *Sostdc1* high affinity binding sites in a dosage-dependent manner. Together, these findings confirm that the high affinity HOXA13 binding site deduced by quantitative analyses is used *in vivo* to facilitate HOXA13 target gene regulation, providing a critical advance toward understanding the molecular basis for defects associated with the loss of HOXA13 function.

Although vertebrate *Hox* genes represent some of the longest studied developmental genes, the molecular basis for their loss of function phenotypes has been difficult to establish. One explanation for this lack of mechanistic progress is that the developmental functions of HOX proteins are inextricably linked to the biophysical properties of the native proteins, including the composition of their preferred binding sites, affinity for these sites, and the effects of interacting proteins. When the DNA binding properties of HOX proteins have been characterized, significant advances in interpreting their developmental functions have occurred (1–3). Key to this functional characterization is the emerging concept that HOX proteins utilize binding sites longer than the canonical TAAT motif, a process facilitated both by the intrinsic amino acid composition and structure of the full-length protein as well as extrinsic interactions with members of the PBC and MEIS classes of TALE proteins (4–10).

Mutations in *Hoxa13* cause hand-foot-genital syndrome, an autosomal dominant disorder that causes preaxial digit loss, reduced carpal/tarsal chondrogenesis, and a loss of interdigital programmed cell death (11). This syndrome has been successfully modeled in mice, where mutations similar to those causing hand-foot-genital syndrome also affect preaxial digit formation, carpal and tarsal element chondrogenesis, and interdigital programmed cell death (12–14). Examining the mechanisms for the loss of programmed cell death in *Hoxa13* mutant limbs, we identified several gene-regulatory elements in *Bmp2* and *Bmp7* that were bound by HOXA13 (14). Expanding these initial studies, we first focused on identifying the DNA sequences bound by HOXA13 with high affinity. By coupling biochemical site selection with a quantitative assessment of HOXA13 DNA binding affinity, the full-length binding site for HOXA13 was determined. Quantitation of HOXA13 affinity for this site, AAATAAAAC, revealed high affinity (3.8 nM), a finding contrasted by similar studies of HOXA1 that suggested only weak binding to DNA (15).

Next, to draw a functional correlation between the HOXA13 binding site and the defects present in *Hoxa13* mutant limbs, we examined whether genes exhibiting perturbed expression in the mutant limb contained high affinity binding sites in their gene regulatory regions. By this analysis, we identified multiple HOXA13 binding sites within two genomic regions flanking the BMP antagonist, *Sostdc1*, whose expression in the limb was previously unreported (16, 17). This finding, in conjunction with elevated *Sostdc1* expression in *Hoxa13* homozygous mutant limbs, led us to hypothesize that HOXA13 utilizes its unique binding site to suppress *Sostdc1* in the limb and facilitate appropriate levels of BMP signaling. Testing this hypothesis, we confirmed that *Bmp4*, *Bmp5*, and *Bmp7* expression were normally expressed in regions ectopically expressing *Sostdc1*; however, in these same regions, BMP signaling throughput was substantially reduced, suggesting that ectopic levels of SOSTDC1 in *Hoxa13* mutant limbs were antagonizing BMP-mediated signaling. SMAD phosphorylation in the ectopic *Sostdc1* regions was also reduced, confirming that BMP signaling throughput was reduced in *Hoxa13* mutant limbs irrespec-

* This work was supported by grants from the Shriners Hospital for Children (to H. S. S. and H. P. B.), National Institutes of Health Grants 5R01DK066539-01 (to H. S. S.) 5T32GM008617-09 (to W. M. K.), and an N. L. Tartar Research Fellowship (to W. M. K.). Biostatical and Affymetrix microarray support was provided in part by the Biostatistics Shared Resource of the Oregon Health and Science University Cancer Institute (Grant P30 CA69533). The costs of publication of this article were defrayed in part by the payment of page charges. This article must therefore be hereby marked "*advertisement*" in accordance with 18 U.S.C. Section 1734 solely to indicate this fact.

[S] The on-line version of this article (available at http://www.jbc.org) contains supplemental Fig. 1 and Tables 1 and 2.

[1] To whom correspondence should be addressed: Shriners Hospital for Children, 3101 S.W. Sam Jackson Park Rd., Portland, OR 97239. Tel.: 503-221-3447; E-mail: hss@shcc.org.

tive of normal *Bmp4*, *Bmp5*, and *Bmp7* expression in these same tissues. *In vivo*, HOXA13 binds the *Sostdc1* locus in the limb at two conserved regions. *In vitro*, HOXA13 can utilize multiple DNA binding sites within these bound sequences to suppress gene expression in a dosage-dependent manner. Together, these findings demonstrate that the HOXA13 binding site elucidated by quantitative methods is used *in vitro* and *in vivo* to regulate target gene expression, providing a mechanism to help explain the molecular basis for malformations associated with the loss of HOXA13 function.

EXPERIMENTAL PROCEDURES

Selection of the HOXA13 Binding Site from Random DNA Sequences—The A13-DBD[2] peptide used for DNA binding assays was generated as previously described (14). For the SELEX enrichment screen, a library of randomized 52-bp double-stranded DNA fragments was generated by PCR using an oligonucleotide containing fixed 5′ and 3′ amplification sequences and 16 random nucleotides (N_{16}) as a core sequence: TACGTCGAATTCGTCAGTN$_{16}$GATGGATCCTGATGTAGA-3′. Coupling efficiency-adjusted phosphoramadite concentrations were used during oligonucleotide synthesis to ensure complete randomization of the N_{16} core nucleotides as described by the manufacturer (Integrated DNA Technologies). Generation of the double-stranded DNA SELEX library was achieved by PCR and the following forward and reverse primers: R16F, 5′-TACGTCGAATTCGTCAGT-3′; R16R, 5′-TCTACATCAGGATCCATC-3′. Amplified double-stranded DNA was radiolabeled by T4 polynucleotide kinase in the presence of [γ-^{32}P]dATP (4500 Ci/mmol; MPBio). ^{32}P-Labeled DNA sequences were then incubated with 0.5 μM A13-DBD peptide, and electrophoretic mobility shift assay was performed as previously described (14). The A13-DBD-bound DNA fragments were excised from the gel and eluted by 2 h of incubation at 65 °C in DNA buffer (50 mM Tris-HCl, pH 8.4, 1 mM EDTA, 0.5% Tween 20). Eluted DNA was purified using a Sephadex G-25 column, amplified using R16F and R16R primers, and used for the next cycle of selection. After a total of five rounds of selection and amplification, the eluted DNA was cloned into the pt3t7 vector and transformed into TOP10 *Escherichia coli* (Invitrogen), and the cloned regions were sequenced and analyzed using VectorNTI (InforMax, Inc.). Energy-normalized LOGOS plots were generated using the EnoLOGOS Web tool (18); the height of each represented base is weighted based on its frequency at a given position within the 100 aligned SELEX sequences.

Fluorescence Anisotropy—The 63-amino acid HOXD13 homeodomain peptide (D13-DBD) (GRKKRVPYTKLQLKELENEYAINKFINKDKRRRISAATNLSERQVTIWFQNRRVKDKKIVSKC) was synthesized and purified as previously described for the A13-DBD (14). Fluorescence anisotropy measurements were performed on a Pan Vera Beacon 2000 fluorescence anisometer (Invitrogen). Self-annealing oligonucleotides were synthesized carrying a fluorescein via a hexyl linker (6-carboxyfluorescein) at the 5′ end and purified by high pressure liquid chromatography (Integrated DNA Technologies). Oligonucleotide sequences are presented in supplemental Table 1. Oligonucleotides were resuspended as a 100 μM stock in Tris-EDTA buffer, diluted to 100 nM in Annealing Buffer (1 M NaCl, 10 mM Tris-HCl, 0.1 mM EDTA, pH 8), denatured at 95 °C for 10 min, and annealed by cooling to room temperature for 30 min. Increasing amounts of A13-DBD peptide (0–200 nM) were added to a solution containing 2 nM fluorescein-labeled DNA in 20 mM Tris, pH 7.5, 80 mM KCl, 10 mM $MgCl_2$, 0.2 mM EDTA, 1 mM dithiothreitol, and incubated at 15 °C for 1 h. Measurements were collected at 15 °C with a 10-s delay. For each protein concentration, three independent binding assessments were performed, and the values were averaged in order to determine the dissociation constants and S.D. values. The following nonlinear least squares fit equation was used to plot the anisotropy data and to calculate the HOXA13-DNA association constant (K_a),

$$A = \frac{1 + K[\mathrm{P}] + K[\mathrm{DNA}] - \sqrt{(1 + K[\mathrm{P}] + K[\mathrm{DNA}])^2 - 4[\mathrm{P}][\mathrm{DNA}]K^2}}{2K[\mathrm{DNA}]} \times (A_m - A_0) + A_0 \quad \text{(Eq. 1)}$$

where A represents anisotropy value, A_m is maximum anisotropy value detected, A_0 is minimum anisotropy value detected (anisotropy without protein), K is K_a, [P] is protein concentration, and [DNA] is DNA concentration fixed at 1 nM. The dissociation constants were calculated using the formula $K_d = 1/K_a$.

Full-length HOXA13 Expression and Purification—The *Hoxa13* cDNA was cloned into the pET16b expression plasmid and transformed into Rosetta2 *E. coli* (Novagen). HOXA13 expression was induced with the addition of 100 mM isopropyl 1-thio-β-D-galactopyranoside for 1 h, cells were collected by centrifugation and lysed in B-Per (Pierce), and the cell pellet was solubilized in 6 M guanidine HCl, 300 mM NaCl, 50 mM sodium phosphate, pH 7. The AthenaES Protein Folding Buffer 6 (50 mM MES, pH 6, 240 mM NaCl, 10 mM KCl, 1 mM EDTA, 0.5 M arginine, 0.4 M sucrose, 0.5% Triton X-100, 0.5% polyethylene glycol 3550, 1 mM GSH, 0.1 mM GSSH) was identified using the AthenaES protein refolding kit to screen for buffers compatible with refolding the denatured His-HOXA13. His-HOXA13 was then purified using TALON beads (Clontech) according to the manufacturer's protocol with the following modification. Purified protein was eluted in Folding Buffer 6 containing 250 mM imidazole. Purified protein was dialyzed into Folding Buffer 6 to remove imidazole and quantitated by amino acid analysis.

In Situ Hybridization—The antisense riboprobe specific for *Hoxa13* was produced as described (19). The 450-bp *Sostdc1* riboprobe was generated using the primers SostF (5′-AACAGCACCCTGAATCAAGC-3′) and SostR (5′-TCTCTTCCGCTCTCTGTGGT-3′) and amplified by PCR from E12.5 embryonic cDNA. The rabbit anti-phosphorylated SMAD1/5/8 antibody was used at a 1:1000 dilution. Whole mount *in situ*

[2] The abbreviations used are: A13-DBD, HOXA13 DNA-binding domain peptide; MES, 4-morpholineethanesulfonic acid; PSMAD1/5/8, phosphorylated SMAD proteins 1, 5, and 8; qRT-PCR, quantitative reverse transcription-PCR; SELEX, systematic evolution of ligands by exponential enrichment; D13-DBD, HOXD13 DNA-binding domain peptide; ChIP, chromatin immunoprecipitation; GFP, green fluorescent protein; PIPES, 1,4-piperazinediethanesulfonic acid; E*x*, embryonic day *x*.

hybridization, immunohistochemistry and confocal imaging of limb frozen sections were performed as previously described (19, 20).

Quantitative RT-PCR—Hoxa13 wild-type and homozygous mutant E14.5 forelimb digit I regions were microdissected in diethyl pyrocarbonate-treated phosphate-buffered saline and snap frozen on dry ice. Six microdissected tissues were pooled for total RNA isolation using RNA STAT-60 as per protocol (Tel-Test). First strand cDNA was synthesized using 2.5 μg of total RNA according to the manufacturer's protocol (ImPromII Reverse Transcription System; Promega). Three independent samples of each genotype (*Hoxa13* wild-type or homozygous mutant) were used for quantitative reverse transcription-PCR (qRT-PCR) analyses with the SYBR Green PCR Master Mix (Applied Biosystems) on an Applied Biosystems model 7700 Sequence Detector thermal cycler and normalized to either *Actin* or *Gapdh* expression. The oligonucleotide sequences of the primers used are found in supplemental Table 2.

Chromatin Immunoprecipitation—Chromatin immunoprecipitation (ChIP) assays were performed using an anti-HOXA13 antibody and a ChIP assay kit (Upstate Biotechnology) as previously described (14), with the following modifications. Cross-linked tissues were lysed in 100 μl of cell lysis buffer (5 mM PIPES, pH 8.0, 85 mM KCl, 0.5% Nonidet P-40) containing 15 μl/ml protease inhibitor mixture (Sigma) and incubated on ice for 10 min. Lysates were centrifuged at 2300 $\times$ g for 5 min at 4 °C, and nuclei were resuspended in 50 μl of nuclei lysis buffer (50 mM Tris-HCl, pH 8.1, 10 mM EDTA, 1% SDS), including 15 μl/ml protease inhibitor mixture and incubated on ice for 10 min. Lysates were sonicated for 10 cycles of 30 s "on" and 1 min "off" at 4 °C using a Bioruptor (Cosmo Bio) to an average length of 200–1000 bp. The chromatin was precleared with 40 μl of salmon sperm DNA/protein A-agarose (Upstate Biotechnology) for 1 h at 4 °C and then centrifuged at 100 $\times$ *g* for 1 min. The protein A-agarose-antibody-HOXA13-chromatin complexes were washed five times with 500 μl of wash buffers (Upstate Biotechnology). After elution and reversing cross-links, chromatin was precipitated with 2.5 volumes of ethanol and incubated at −20 °C for 1 h, and the pellet was dissolved in 100 μl of TE (10 mM Tris·HCl, 1 mM EDTA, pH 8.0). Chromatin was treated with 25 μl of 5× PK buffer (50 mM Tris-HCl, pH 7.5, 25 mM EDTA, 1.25% SDS) and 2 μl of proteinase K (20 mg/ml) per sample and incubated at 55 °C for 1 h. Chromatin was purified using the Qiaquick PCR cleanup kit (Qiagen). Eluted DNA from the antibody, control IgG, and no antibody ChIP samples and from the input chromatin was assessed for the presence of the Sost5′ and Sost3′ DNA regions using PCR and the following primers: Sost5′F, 5′-CCAGACGGTGACAGCACTTA-3′; Sost5′R, 5′-GCATTCTGCATGTCTCTTGC-3′; Sost3′F, 5′-CAGGGCCTACATAGTAGGTA-3′; Sost3′R, 5′-CAATTAGTATAGTTAGCAATTAAC-3′.

Luciferase Reporter Constructs—The 5′ and 3′ regions from the *Sostdc1* locus (NCBI M35 mouse assembly; ENSMUSG00000036169) were identified as conserved regions containing multiple high affinity HOXA13 binding sites. The 5′ region, Sost5′FL, containing five high affinity HOXA13 binding sites was identified at positions −1763 to −495 upstream of the *Sostdc1* initiation codon (see Fig. 5, *B* and *D*). This region was amplified from mouse genomic DNA using PCR with the primers Sost5′F1 (5′-TCCCGACACCATCTTGTTTT-3′) and Sost5′R1 (5′-GTGTAGGGCTTCGGAGTGAA-3′), followed by restriction digest with BglII. The 3′ Sostdc1 region containing 10 HOXA13 binding sites, Sost3′FL, was amplified using the primers Sost3′F1 (5′-CAGTTGGAAGGGTCTGTGGT-3′) and Sost3′R1 (5′-GGCTTCCCACGGTAGAGATT-3′). The Sost3′FL region is downstream of the initiation codon (+1) between bp 5410 and 6912 (see Fig. 5, *B* and *D*). The PCR-amplified Sost5′FL and Sost3′FL products were cloned into the EcoRV site of the pGL4.10 luciferase vector, which is designed to measure the promoter activity of introduced DNA sequences (Promega). The pGL4.10 plasmids containing the Sost5′FL and Sost3′FL fragments are designated pGL4Sost5′FL and pGL4Sost3′FL, respectively. Deletion constructs removing the high affinity HOXA13 binding sites were produced by restriction digests of the pGL4Sost5′FL and pGL4Sost3′FL reporter plasmids. The Sost5′Δ1 construct was produced by a Hind III restriction digest, which removed bp −1066 to −495 and ablated three of the five HOXA13 binding sites in the Sost5′FL element. Sost3′Δ1 was subcloned from the pGL4Sost3′FL plasmid by sequential restriction digests with PpuMI and BglII, which removed bases 6583–6912 and six of the 10 HOXA13 binding sites. The Sost3′Δ2 deletion was produced by sequential restriction digests with NdeI and BglII, which removed bases 5864–6912, ablating all 10 high affinity HOXA13 binding sites. The sequences and orientation of all cloned fragments were verified by sequencing (ABI).

Luciferase Assays—NG108-15 cells (ATCC HB-12317) were maintained and transfected as previously described (14). Transfections were performed in 12-well plates (Costar) using 2 μg of pGL4 plasmid, 0.25 μg of pRL-CMV *Renilla*, and 0.125–0.5 μg of pCAGGS-*Hoxa13* or empty pCAGGS control plasmid per well. Cell lysates were processed to detect luciferase activity using the Dual-Glo Luciferase Assay System (Promega) in Opti-Plate-96F black plates (Packard) as described (Promega) (14). Luciferase activity was detected using a Packard Fusion Microplate Analyzer (PerkinElmer Life Sciences), and wells were read three times for 1 s each and averaged. Two replicates of each transfection were performed, and each transfection assay was repeated three times. Results were normalized for *Renilla*, and control transfections were set to an relative luciferase unit value of 100 and plotted using SigmaPlot 9.0 (Systat).

RESULTS

The HOXA13 core binding sequences were identified using a systematic evolution of ligands (SELEX) site selection screen (21). A library of randomized, double-stranded oligonucleotides were incubated with saturating amounts (500 nM) of the HOXA13 DNA binding domain peptide (A13-DBD) (Fig. 1*A*) (14). DNA sequences exhibiting reduced electrophoretic mobility due to A13-DBD binding were isolated and subjected to five consecutive rounds of binding and electrophoretic enrichment (Fig. 1*B*). One hundred independent sequences selected by this process were examined using Vector NTI software (InforMax, Inc.) which revealed a core sequence of TAA in all of the bound sequences (Fig. 1, *C* and *D*). Analysis of the flanking base composition revealed 50% of the A13-DBD bound

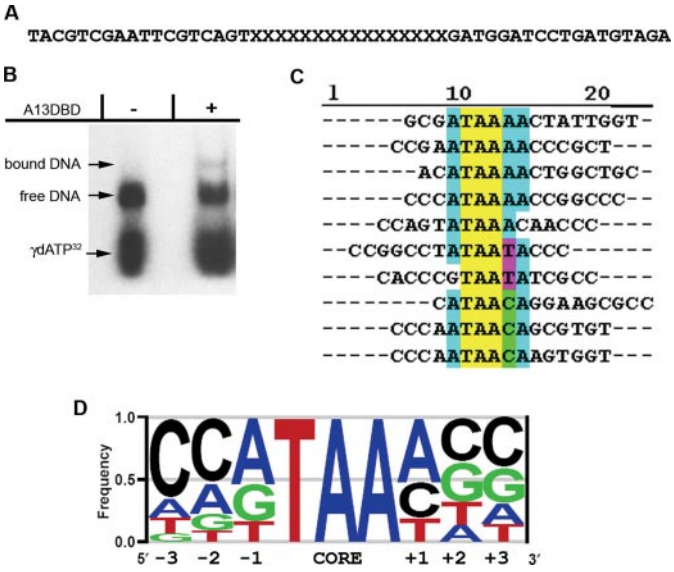

FIGURE 1. **Identification of HOXA13 DNA binding sites.** *A*, the randomized DNA sequence used for DNA binding selection. *B*, electrophoretic mobility shift assay of A13-DBD peptide bound to DNA sequences present in the first round of DNA binding selection. Bound DNA, free DNA, and [γ-^{32}P]dATP are labeled (*arrows*). *C*, alignment of 10 representative DNA sequences bound by A13-DBD after five rounds of selection. Core DNA sequence motifs are *highlighted*. *D*, energy-normalized logo (EnoLOGOS) plot of the A13-DBD binding site derived from 100 selected and aligned DNA sequences. The *height* of each represented base is weighted based on its frequency at a given position within the 100 aligned SELEX sequences.

TAA-containing sequences were TAAA, 30% were TAAC, and 20% were TAAT, suggesting that HOXA13 may utilize three separate core binding sites to regulate target gene expression (Fig. 1, *C* and *D*).

Next, because the nucleotides flanking the transcription factor core binding sites play a critical role in determining transcription factor-DNA affinity and can be misrepresented by the saturating protein concentrations used in SELEX screens (22–24), we performed a series of fluorescence polarization affinity analyses to determine which nucleotides flanking the TAA core confer the highest A13-DBD binding affinity (Fig. 2*A*). Starting with an initial sequence CCA**TAA**ACC, as identified by the SELEX alignment (Fig. 1*D*), the nucleotides flanking the core TAA site (3 bp upstream and 3 bp downstream) were queried for their affects on A13-DBD binding affinity. Altering the nucleotide composition at any of the six positions flanking the core binding site resulted in substantial changes in A13-DBD binding affinity (Fig. 2, *B*–*G*). Notably, changes at positions −2, −1, and +1 had the greatest affect on A13-DBD binding affinity (Fig. 2, *C*–*E*). For the −2-position, the replacement of the favored A nucleotide with a G results in a 16-fold decrease in binding affinity (ΔK_d = 5.4 ± 0.6 to 86 ± 11 nM) (Fig. 2*C*). Similarly, the replacement of the A nucleotide with a C at the −1 position also altered the A13-DBD affinity, causing a 16-fold reduction (ΔK_d = 9.4 ± 0.2 to 154 ± 34 nM) (Fig. 2*D*). At the +1-position, A13-DBD binding affinity varied from the canonical TAAT sequence reported for other homeodomains (7), preferring an A in this position, which increased A13-DBD affinity 10-fold (Fig. 2*E*). Strikingly, even base changes at the −3- and +3-positions outside the TAA core affect A13-DBD binding affinity 3–7-fold (Fig. 2, *B* and *G*).

Assessing the quantitative affects of all nucleotide substitutions on A13-DBD DNA binding affinity revealed a predicted high affinity consensus sequence of AAATAAAAC (Fig. 2*H*). Analysis of A13-DBD binding to this predicted consensus sequence resulted in the highest affinity DNA binding detected, with a K_d of 3.9 ± 0.3 nM (Fig. 3, *A* and *B*). Interestingly, HOXD13, the closest paralog of HOXA13, exhibited nearly 15-fold less affinity for this same sequence (K_d = 56 ± 0.1 nM), suggesting high specificity for HOXA13 binding to this consensus site (Fig. 3*B*). In addition, we confirmed that the full-length HOXA13 protein also binds this same sequence with an affinity identical to the A13-DBD peptide (K_d = 3.6 ± 0.5 *versus* 3.9 ± 0.3 nM), validating the modular function of the HOXA13 DNA binding domain (Fig. 3*C*).

A major goal for identifying the high affinity HOXA13 binding sites was to provide a mechanism to identify genes directly regulated by HOXA13 and to correlate this regulation with malformations associated with the loss of *Hoxa13* function. Using high density microarrays (Affymetrix), the gene expression profiles present in E12.5 *Hoxa13* wild-type and homozygous mutant autopods were compared (data not shown). Knowing that HOXA13 regulates *Bmp2* and *Bmp7* expression in the autopod (14), we focused our analysis of the microarray data to genes belonging to the BMP signaling pathway.

From this analysis, a greater than 2-fold increase in the expression of the BMP antagonist *Sostdc1* (*Ectodin*, AB059271) was detected in E12.5 *Hoxa13* homozygous mutant limbs. The presence of *Sostdc1* in the limb as well as its overexpression in *Hoxa13* mutant limbs was surprising, since previous characterizations of *Sostdc1* reported the tooth bud and kidney as the predominant regions of expression and loss of function phenotype (16, 17, 25).

To validate that *Sostdc1* is expressed in the limb and to identify the mutant limb regions overexpressing *Sostdc1*, *in situ* hybridization of E12.5–E14.5 embryos was performed using a *Sostdc1* riboprobe. The localization of *Hoxa13* and *Sostdc1* transcripts in wild-type limbs revealed reciprocal domains of expression (Fig. 4, *A*–*F*). At E12.5, *Hoxa13* is expressed in the autopod mesenchyme, whereas *Sostdc1* is expressed in the distal zeugopod, which does not express *Hoxa13* (Fig. 4, *A* and *D*). At E13.5, the transition of *Hoxa13* expression to the digits is coincident with the appearance of *Sostdc1* expression in the interdigital tissues and distal zeugopod, where *Hoxa13* is not expressed (Fig. 4, *B* and *E*). At E14.5, *Hoxa13* is strongly expressed in the ventral autopod, particularly in digit I, the phalangeal joints, and the developing footpads, whereas *Sostdc1* expression is excluded from these same domains (Fig. 4, *C* and *F*).

In contrast, *Hoxa13* mutant limbs exhibit expanded *Sostdc1* expression into the proximal *Hoxa13* expression domain of the autopod as early as E12.5 (compare Fig. 4, *A*, *D*, and *G*). In E13.5–E14.5 mutant limbs, *Sostdc1* expression is also elevated in the ventral digit I domain as well as in the developing footpads, tissues where *Hoxa13* is normally expressed (Fig. 4, *E*, *F*, *H*, and *I*). To quantitate the expression differences detected by *in situ* hybridization, qRT-PCR was performed using RNA isolated from the affected ventral limb domain (Fig. 4, *J* and *K*). A comparison of *Sostdc1* expression in wild-type and homozy-

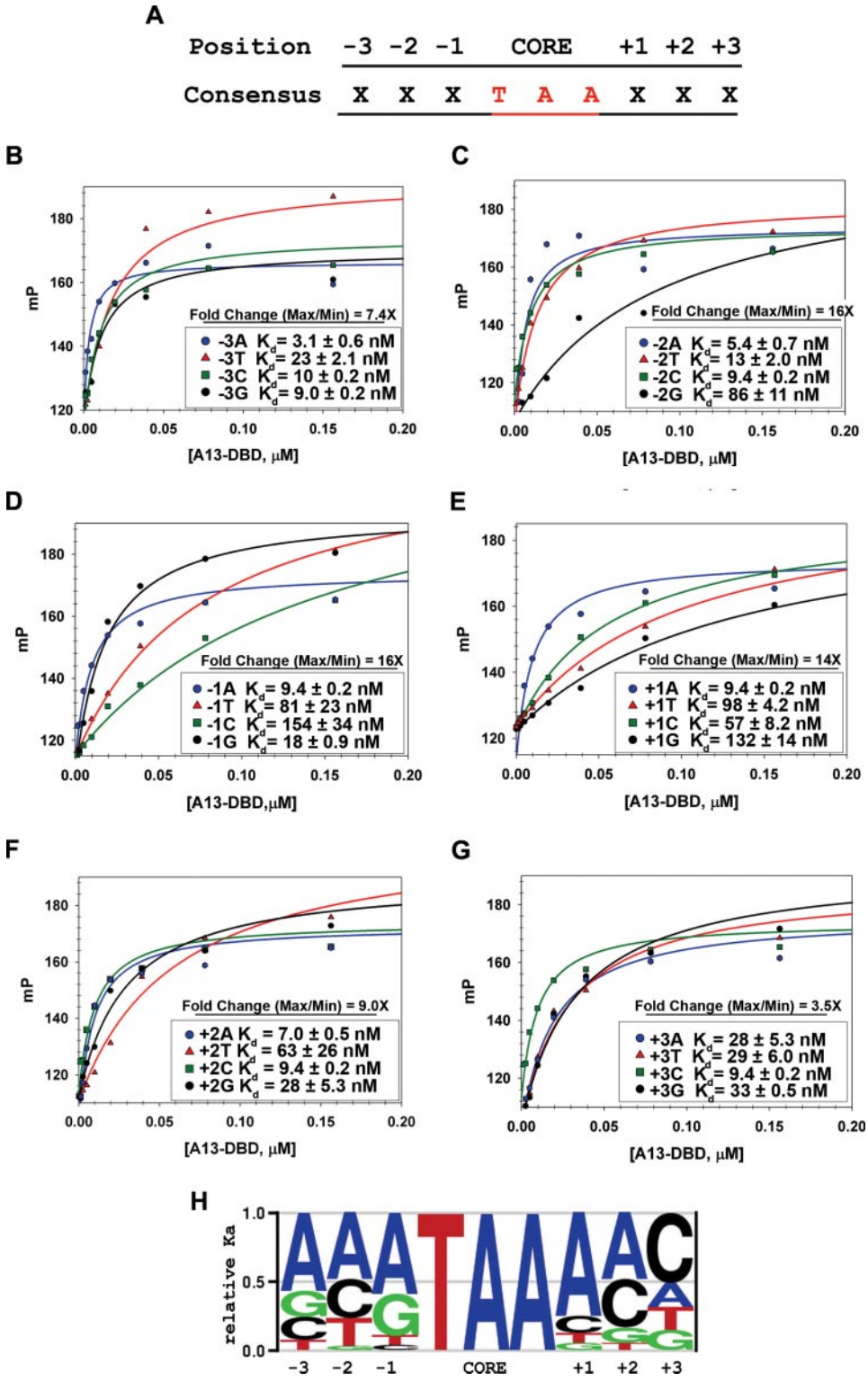

FIGURE 2. **Quantitation of HOXA13 DNA binding affinity.** *A*, the DNA sequence used for quantitative analysis of A13-DBD binding, *X* indicates an A, T, C, or G at that position. *B–G*, fluorescence polarization analyses with base substitutions at positions −3 (*B*), −2 (*C*), −1 (*D*), +1 (*E*), +2 (*F*), and +3 (*G*) of the DNA sequence in *A*. *H*, EnoLOGOS plot of the A13-DBD high affinity DNA sequence derived from the K_d values depicted in *B–G*. The *height* of each represented base is weighted using the association constant (K_a) of A13-DBD at each position within the sequence. Anisotropy data points represent the average of three independent measurements at each protein concentration. Plots represent a nonlinear least squares fit of the data. *Error bars* have been omitted to facilitate direct comparisons between plots. The dissociation constant (K_d) for each plot is represented in the *boxed legend* followed by its S.D. value.

gous mutant limbs confirmed a consistent 2-fold increase in expression in the mutant limb ($n = 3$ independent analyses) (Fig. 4*K*). Analysis of the *Bmp* genes expressed in the ectopic *Sostdc1* domain revealed *Bmp4*, *Bmp5*, and *Bmp7* expression within digit I and the footpad region; however, *Bmp2* expression was not detected in these same tissues at E14.5 (Fig. 4*K*; data not shown). qRT-PCR analysis revealed no differences in *Bmp4*, *Bmp5*, or *Bmp7* expression between wild-type and homozygous mutant digit I and footpad tissues (Fig. 4*K*).

Using VISTA plot analysis (26) to identify conserved gene-regulatory sequences within the murine *Sostdc1* locus, we identified conserved regions 5′ (Sost5′FL) and 3′ (Sost3′FL) of *Sostdc1* that contained multiple high affinity HOXA13 binding sites (Fig. 5, *A*, *B*, and *D*). Analysis of these regions revealed high conservation among several vertebrate species, including mouse (*Mus musculus*), rat (*Rattus norvegicus*), dog (*Canis familiaris*) and human (*Homo sapiens*) (Fig. 5*B*) (27). To assess whether HOXA13 binds the Sost5′FL and Sost3′FL sites *in vivo*, a ChIP assay was used to identify HOXA13-DNA complexes present in the developing limb. The HOXA13 antibody used in the ChIP assay is capable of immunoprecipitating both wild-type HOXA13 and mutant HOXA13-GFP proteins (14). ChIP analysis of wild-type limb bud chromatin confirms that HOXA13 associates with both *Sostdc1* sites *in vivo* in the developing limb (Fig. 5*C*). In contrast, parallel assays using chromatin derived from homozygous mutant limbs could not detect association between the mutant HOXA13-GFP protein and these same sites, confirming that the DNA binding domain deleted in the mutant HOXA13-GFP protein (13) is essential for HOXA13-DNA association at the Sost5′FL and Sost3′FL sites (Fig. 5*C*).

Based on the ectopic expression of *Sostdc1* in *Hoxa13* mutant limbs as well as the association of

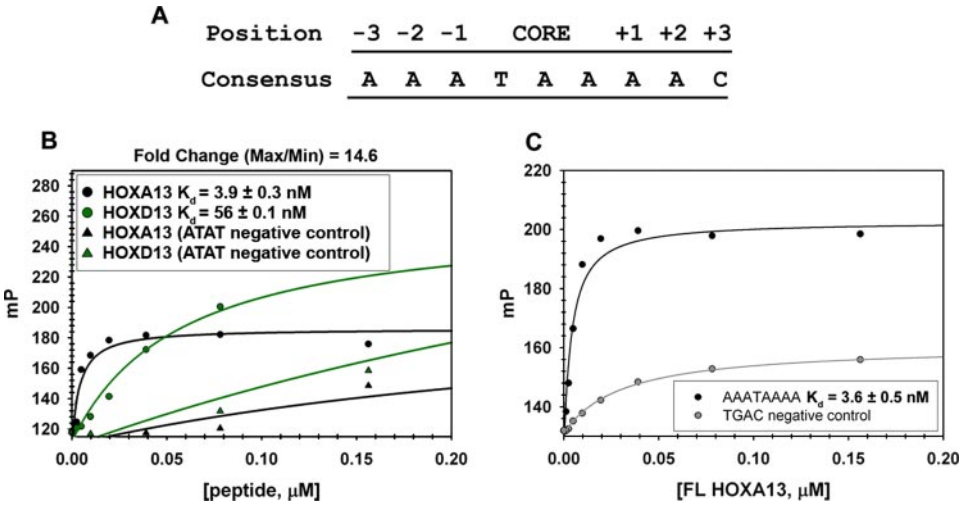

FIGURE 3. **Affinity and specificity analysis of the deduced HOXA13 DNA binding site.** *A*, the high affinity HOXA13 DNA binding site deduced from the fluorescence anisotropy series in Fig. 2. *B*, analysis of A13-DBD affinity for the HOXA13 binding site *versus* a control DNA sequence (*black curves* and *data points*). Specificity was assessed using a HOXD13 DNA binding domain peptide incubated with the same high affinity and control sequences (*green curves* and *data points*). *C*, full-length HOXA13 protein exhibits the same affinity for the high affinity site as the A13-DBD peptide. All anisotropy data points represent the average of three independent measurements at each protein concentration. Plots represent a nonlinear least squares fit of the data. Error bars have been omitted to facilitate direct comparisons between plots. The dissociation constant (K_d) for each plot is represented in the *boxed legend* followed by its S.D. value.

HOXA13 with the Sost5′FL and Sost3′FL regions *in vivo*, we hypothesized that these sites are bound by HOXA13 to suppress gene expression *in vivo*. Testing this hypothesis *in vitro*, we examined whether luciferase reporter expression directed by the Sost5′FL or Sost3′FL gene-regulatory elements could be suppressed by HOXA13. Transfections with increasing amounts of a HOXA13 expression plasmid (125, 250, and 500 ng) suppressed pGL4Sost5′FL luciferase expression in a dose-dependent manner, resulting in a 2.5-fold reduction in reporter expression compared with the control (Fig. 5*E*). Removing three of the five HOXA13 binding sites in the Sost5′FL element (Sost5′Δ1) reduced the capacity of HOXA13 to suppress luciferase expression regardless of the dosage of the HOXA13 plasmid (Fig. 5*F*). Luciferase reporter constructs containing the 3′ *Sostdc1* regulatory element, pGL4Sost3′FL, also responded to increasing amounts of HOXA13, suppressing luciferase expression 4-fold compared with controls (Fig. 5*G*). Removal of six of the 10 HOXA13 binding sites in the Sost3′FL element (Sost3′Δ1) caused a similar reduction in the capacity of HOXA13 to suppress luciferase expression (Fig. 5*H*). The removal of all 10 HOXA13 binding sites in the Sost3′FL element (Sost3′Δ2) completely negated the capacity of HOXA13 to suppress reporter expression, confirming that HOXA13 utilizes these high affinity binding sites to suppress gene expression *in vitro* (Fig. 5*I*).

The transduction of BMP signaling is facilitated by receptor-mediated SMAD1/5/8 phosphorylation and induced target gene expression (28). Previous studies using ectopic SOSTDC1 confirm its function as a potent BMP antagonist inhibiting BMP-induced osteoblast differentiation *in vitro* as well as BMP-mediated target gene expression in the developing tooth cusp (16). These findings in conjunction with previous reports that ectopic NOGGIN can affect the differentiation of the condensed digit mesenchyme (29, 30) led us to hypothesize that ectopic *Sostdc1* expression in *Hoxa13* mutant limbs would cause a similar reduction in BMP-mediated gene expression and SMAD phosphorylation.

Immunohistochemistry using a phosphorylation-specific SMAD1/5/8 antibody revealed strong SMAD1/5/8 phosphorylation in the wild-type E14.5 autopod (Fig. 6, *A* and *C–E*). In the dorsal digit I-II region, phospho-SMAD1/5/8 staining is present primarily in the interdigital tissues (Fig. 6, *C* and *D*, *white arrows*). In the ventral autopod, SMAD1/5/8 staining is also detected in the perichondrial region of digit I (Fig. 6*E*, *white arrowhead*) as well as the developing footpad (Fig. 6*E*, *white asterisks*). In contrast, age-matched *Hoxa13* homozygous mutants exhibit reduced levels of SMAD1/5/8 phosphorylation in the domains overexpressing *Sostdc1*, including the interdigital tissues (Fig. 6, *B*, *F*, and *G*, *white arrows*) as well as the ventral digit I/footpad domain (Fig. 6, *F–H*, *white arrowheads*/*white asterisks*).

This reduction in SMAD1/5/8 phosphorylation prompted us to investigate whether BMP-regulated target genes were also misexpressed in the ectopic *Sostdc1* domain.

qRT-PCR analysis using RNA isolated from the ectopic *Sostdc1* domain confirms that BMP target genes are down-regulated in *Hoxa13* homozygous mutants, including *Msx1* (−3-fold), *Collagen type II* (−3-fold), *Collagen type X* (−2.5-fold), *Sox9* (−3.5-fold), and *Ihh* (−1.7-fold) (Fig. 6*I*). Interestingly, some putative BMP target genes did not exhibit reduced expression, including *Msx2*, *Id2*, *Mfh1*, *Bambi*, and *Runx2*, suggesting that BMP-independent processes may also be used to maintain their expression (Fig. 6).

DISCUSSION

HOXA13 function is essential for the normal development of the distal limb and genitourinary tract. Prior to this investigation, mutational studies of HOXA13 have focused on the cellular mechanisms affected by its loss of function, such as defects in cell adhesion, reduced proliferation, and a decrease in programmed cell death (13, 14, 19). In the present study, we sought to extend what was known about HOXA13 developmental function by characterizing its biochemical properties as a transcription factor. From this analysis, we define the DNA sequences bound with high affinity by HOXA13 and confirm their utilization to regulate the expression of the BMP antagonist *Sostdc1*, providing a mechanism to interpret HOXA13 developmental function from a quantitative transcriptional perspective.

A major criticism of SELEX-based site selection is that the predicted sites vary from those used by the transcription factors *in vitro* and *in vivo*. One explanation for this paradox

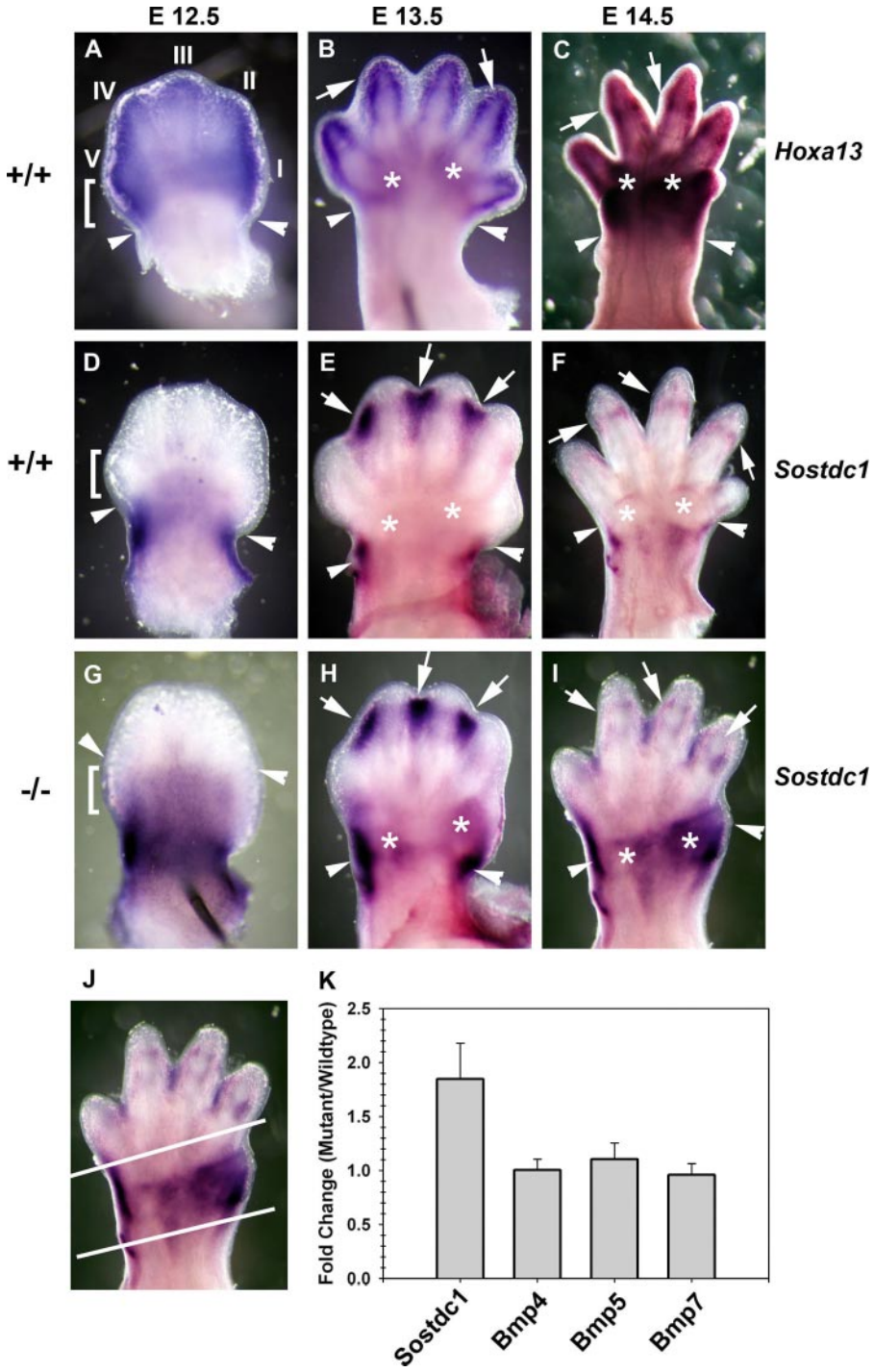

FIGURE 4. **Ectopic *Sostdc1* in HOXA13 mutant autopods correlates with domains of *Hoxa13* expression.** *A–I*, analysis of *Hoxa13* and *Sostdc1* expression in E12.5–E14.5 ventral forelimb autopods by *in situ* hybridization. *A–C*, *Hoxa13* expression in wild-type autopods; proximal expression boundaries are indicated by *white arrowheads*. *A*, *Hoxa13* expression is present throughout the E12.5 ventral autopod; digits I–V are labeled. *B*, at E13.5, *Hoxa13* expression is localized to the peridigital (*white arrows*) and developing footpad (*white asterisks*) tissues. *C*, by E14.5 *Hoxa13* expression is in the developing digits, joints (*white arrows*), and footpad tissues (*white asterisks*). *D–F*, *Sostdc1* expression in wild-type autopods. *D*, at E12.5, *Sostdc1* expression is restricted to the zeugopod. *E*, by E13.5, *Sostdc1* is expressed in the interdigital tissues between digits II and III, III and IV, and IV and V (*white arrows*) as well as the lateral region of the proximal autopod (*white arrowheads*) but not in the developing footpads (*white asterisks*). *F*, *Sostdc1* expression at E14.5 is in discrete bands within digits I–V (*white arrows*) as well as in an expression domain proximal to the developing footpads (*white arrowheads*). *Sostdc1* expression is not detected in the developing footpads (*white asterisks*). *G–I*, *Sostdc1* expression in E12.5–E14.5 *Hoxa13* homozygous mutant autopods. *G*, *Sostdc1* expression at E12.5 has expanded into the autopod (*white arrowheads*) and overlaps with the proximal expression domain of *Hoxa13* (compare *white brackets* in *A*, *D*, and *G*). *H*, in E13.5 autopods, there is ectopic *Sostdc1* expression in the proximal autopod (*white arrowheads*) and in the developing footpads and ventral digit I tissues (*white asterisks*). *Sostdc1* expression is also increased in the interdigital tissues (compare *white arrows* in *E* and *H*). *I*, at E14.5, *Sostdc1* expression is present in the footpads and digit I (*white asterisks*) as well as in the proximal autopod (*white arrowheads*). *Sostdc1* expression persists in the interdigital tissues between digits II and III, III and IV, and IV and V and is expanded in the digits as compared with wild type (compare *white arrows* in *F* and *I*). *J*, *Sostdc1 in situ* of an E14.5 wild-type ventral limb; *white bars* indicate the digit I and footpad region microdissected for qRT-PCR in *K*. *K*, qRT-PCR using E14.5 mRNA isolated from *Hoxa13*$^{+/+}$ and *Hoxa13*$^{-/-}$ digit I tissues, calculated as the -fold change in expression of mutant divided by wild type.

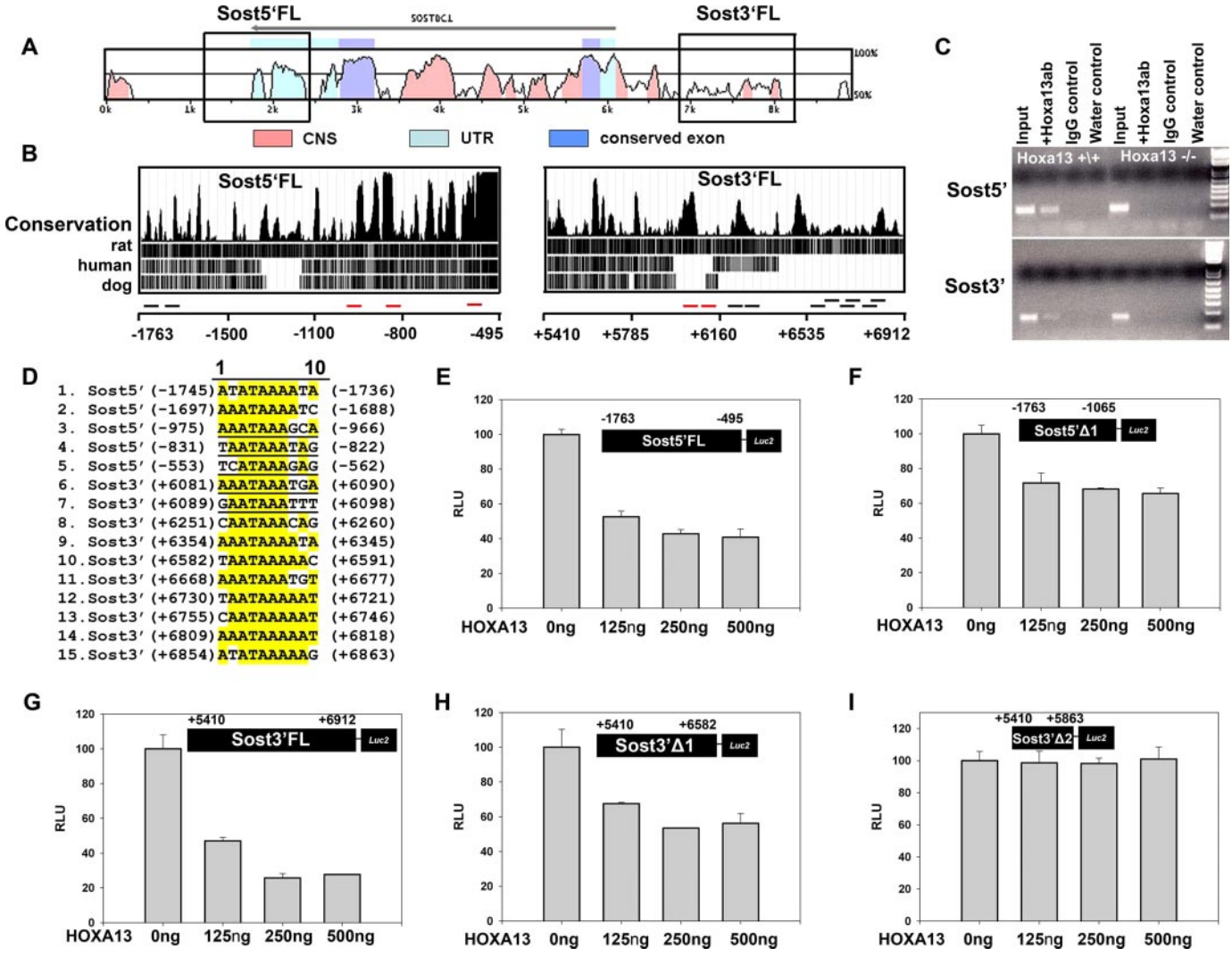

FIGURE 5. **HOXA13 binds DNA sequences in *Sostdc1* to repress gene expression.** *A*, VISTA plot of *Sostdc1* sequence conservation between humans and mice. Gene information is *color-coded* as labeled: *pink*, conserved noncoding sequence (*CNS*); *light blue*, untranslated region (*UTR*); *blue*, conserved exon. *Black boxes* indicate conserved genomic regions containing HOXA13 DNA binding sites 5′ (Sost5′FL) and 3′ (Sost3′FL) of the *Sostdc1* coding sequence. *B*, detailed view of Sost5′FL (*left*) and Sost3′FL (*right*) DNA sequence conservation between mice, rats, humans, and dogs. *C*, ChIP assay of HOXA13 bound to high affinity DNA sequences within Sost5′FL (*top*) and Sost3′FL (*bottom*) genomic regions in E12.5 forelimb autopod tissues. *Hoxa13*$^{+/+}$ (*left lanes*) and *Hoxa13*$^{-/-}$ (*right lanes*) ChIP samples are labeled (input, +Hoxa13 antibody, IgG control, water control). ChIP DNA fragments are only amplified in the input lanes and *Hoxa13*$^{+/+}$ immunoprecipitated samples. *D*, alignment of HOXA13 high affinity binding sites present in Sost5′FL and Sost3′FL. Sequence positions relative to the start codon of *Sostdc1* are indicated for each binding site (*1–15*); binding sites present in the ChIP fragments are *underlined*. *E–I*, luciferase assays in NG108-15 cells using a deletion series of Sost5′ and Sost3′ genomic regions. Relative luciferase units (*RLU*) are indicated on the *y* axis, and the quantity of transfected pCAGGS-*Hoxa13* is labeled on the *x* axis (the 0 ng lane is transfected with 500 ng of empty pCAGGS plasmid as a control). *E*, co-transfection of HOXA13 and Sost5′FL represses luciferase expression 2.5-fold when compared with control pCAGGS transfections. *F*, the truncated Sost5′FLΔ1 is only repressed 1.4-fold. *G*, co-transfection of Sost3′FL and HOXA13 represses luciferase expression 4-fold. *H*, the Sost3′Δ1 truncation is repressed 2-fold, whereas the Sost3′Δ2 truncation relieves the HOXA13 repression (*I*).

is that the protein concentrations used for SELEX often exceed the transcription factor's dissociation constant (K_d), promoting nonspecific protein-DNA interactions, particularly at the nucleotides flanking the core residues (22–24, 31). Thus, at physiological concentrations of a transcription factor, the binding sites predicted using excess protein would not be readily bound. This conclusion is supported by the variations between the HOXA13 binding sites predicted by SELEX, CC(A/G)TAA(A/C/T)(C/G/T)(C/G/A), and the high affinity sites determined by quantitative fluorescence polarization. It is important to note that the AAATAAAAC high affinity site refined by fluorescence polarization does not reflect the sole site that HOXA13 can bind *in vivo*, since some of the sequence variations at positions −3, −2, −1, and +2 caused only a slight increase in the dissociation constant (Fig. 2).

Whereas the HOXA13 core sequence identified as TAAA is similar to other reported HOX binding sites, this core sequence appears unique compared with the TTA(G/C) core sequences bound by other Abd-B proteins, including HOXA10, HOXC13, and HOXD13 (6, 32–34). More importantly, although HOXA10, HOXC13, and HOXD13 appear to bind the same core sequence, the full-length sequences bound by each protein, including HOXA13, vary, suggesting that the disparate phenotypes exhibited by *Hoxa13*, *Hoxa10*, *Hoxc13*, and *Hoxd13* knock-out mice can be explained, in part, by the capac-

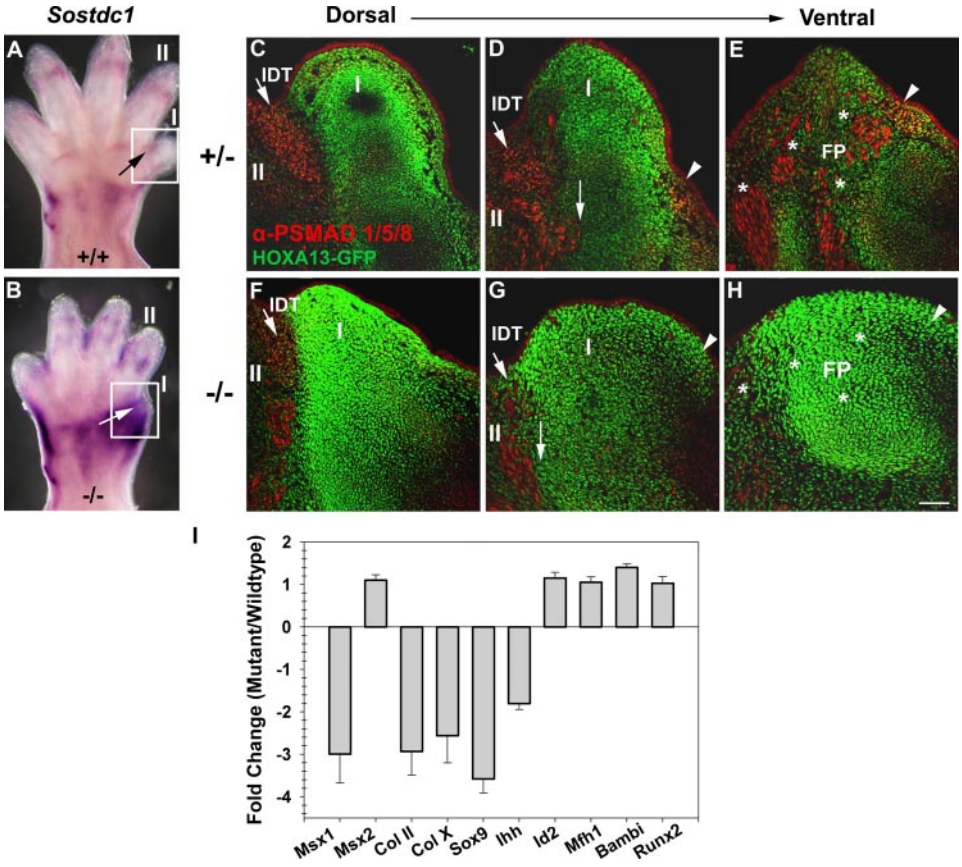

FIGURE 6. **Reduced BMP signaling correlates with ectopic *Sostdc1* in the *Hoxa13* mutant autopod.** *A* and *B*, *Sostdc1* expression in E14.5 *Hoxa13*$^{+/+}$ (*A*) and *Hoxa13*$^{-/-}$ (*B*) ventral forelimbs. The *white boxes* indicate the digit I tissues analyzed in *C–H*; the *arrows* point to the interdigital tissues (*IDT*) between digits I and II. *C–H*, a dorsal to ventral series of frontal frozen sections through *Hoxa13*$^{+/-}$ (*C–E*) and *Hoxa13*$^{-/-}$ (*F–H*) digit I and footpad (*FP*), immunostained with α-PSMAD1/5/8 (*red signal*) and endogenous HOXA13-GFP (*green signal*). Digits I and II and the interdigital tissues are labeled in *white*. *C*, PSMAD1/5/8 staining is present in the interdigital tissues between digits I and II (*white arrow*). *D*, PSMAD1/5/8 staining in the interdigital tissues has expanded within digit I (*white arrows*). *E*, within the footpad, there are multiple domains of PSMAD1/5/8 staining (*white asterisks*). *F*, within *Hoxa13*$^{-/-}$ digit I, there is reduced PSMAD1/5/8 staining in the interdigital tissues (*white arrow*). *G*, PSMAD1/5/8 staining is reduced within *Hoxa13*$^{-/-}$ digit I tissues (compare *white arrows* and *arrowheads* in *D* and *G*). *H*, PSMAD1/5/8 staining is not visible within the *Hoxa13*$^{-/-}$ footpad (compare *asterisks* in *E* and *H*). *I*, qRT-PCR using E14.5 mRNA isolated from the *Hoxa13*$^{+/+}$ and *Hoxa13*$^{-/-}$ digit I and footpad, calculated as the -fold change in mutant divided by wild-type expression. *Bar*, 50 μm.

ity of these proteins to bind discrete gene-regulatory elements (12, 35–37).

HOX protein DNA binding specificity can also be affected by cooperative interactions with other transcription factors (5, 33, 38–40). Notably, interactions between HOX proteins and members of the PBC (PBX1–4, EXD, and CEH-20) and MEIS classes (MEIS-1A and -1B, MEIS2, MEIS3, MEIS4, PREP1, and PREP2) of TALE (three-amino acid loop extension) transcription factors have been shown to modulate HOX protein interaction with specific *cis*-regulatory elements (4, 5, 9, 33, 38–42). For HOXA13, interactions with MEIS1A and MEIS1B have been confirmed *in vitro*, whereas no interactions between HOXA13 and PBC class proteins have been detected, a finding consistent with the absence of a YPWM PBC interaction motif in HOXA13 (4, 9, 33, 38, 39, 41, 43–46).

Recognizing that HOXA13 regulates gene expression in discrete embryonic regions, it is likely that higher order protein complexes containing HOXA13 will augment its gene-regulatory function. Indeed, recent studies confirm that cooperative interactions between HOX proteins, such as HOXB1 and PBX1, can regulate the tissue-specific expression of collagen V (*COLVA2*) (42). In most analyses of HOX-TALE protein interaction, both factors bind DNA to cooperatively regulate gene expression. However, recent studies indicate that TALE factors not bound to DNA can also interact with HOX-TALE heterodimers, forming ternary complexes that affect DNA binding affinity (39, 47).

Although the DNA binding affinity of HOX proteins is usually augmented by cooperative interactions with TALE co-factors, our findings also suggest that HOXA13 may possess monomeric gene-regulatory functions. This conclusion is supported by the strong DNA binding affinity and specificity of the full-length HOXA13 protein for the AAATAAAAC binding site without additional accessory proteins. Moreover, the substantial difference in affinity for the AAATAAAAC site between the HOXA13 and HOXD13 homeodomains, which share greater than 90% amino acid identity, also suggests that properties inherent to the HOXA13 homeodomain may be sufficient to confer this high degree of specificity. Finally, *in vivo* studies of the HOXA13 homeodomain also support the possibility for its independent function, since domain swap experiments replacing the HOXA11 homeodomain with the HOXA13 homeodomain identified transformations of HOXA11-expressing tissues toward those normally expressing HOXA13, including the limb and female reproductive tract (48).

It is arguable that the defects associated with the loss of *Hoxa13* function may reflect early and global perturbations in the condensation of limb mesenchyme. However, because the *Hoxa13* mutant limbs do not exhibit uniform defects in digit chondrogenesis, it is more likely that a region-specific perturbation in the chondrogenic process is occurring, particularly in the digit I domain. An examination of the timing of digit ontogeny supports this conclusion as digit formation in tetrapods proceeds from digit IV to III, to II, to V, and finally to digit I (49–51). Since digit I is the last to form, its maturation at E12.5, as determined by *noggin* expression (supplemental Fig. 1), is consistent with the earliest timing of ectopic *Sostdc1* expression in *Hoxa13* mutant limbs. Similarly, the normal expression of the chondrogenic determinant, *Sox9,* in *Hoxa13* mutant limbs at E11.5 strongly suggests that perturbations in the chondrogenic process are occurring between E11.5 and 12.5 (supple-

mental Fig. 1). These findings in conjunction with the detection of ectopic *Sostdc1* as early as E12.5 in the *Hoxa13* mutant limb strongly suggests that the prochondrogenic processes mediated by BMP signaling could be susceptible to perturbations by an ectopically expressed BMP antagonist.

Studies examining the loss of BMP receptor function after the mesenchymal condensations have formed, confirm that the progression of the chondrogenic process in the limb requires a sustained BMP signal (52, 53). As the limb continues to mature, BMP signaling induces a second round of *Sox9* expression (52). In *Hoxa13* homozygous mutants, this second round of *Sox9* expression is reduced specifically in the ectopic *Sostdc1* expression domain, indicating that the inductive processes normally mediated by BMP signaling are being antagonized, presumably by ectopic SOSTDC1 (supplemental Fig. 1) (54, 55).

In this report, we identify the developing limb as a novel site for *Sostdc1* expression. To date, it is not clear whether SOSTDC1 has a specific function in the limb, since limb defects have not been reported in *Sostdc1* homozygous mutants (17). Here compensatory BMP antagonists may help explain this discrepancy, since both *noggin* and *gremlin* are expressed in these same tissues (30, 51, 56). More importantly, whereas loss of function alleles generally indicate sites requiring a particular protein, they provide little information regarding how ectopic levels of the same protein may affect tissue development. In *Hoxa13* mutant limbs, BMP expression is active in the affected digit I region, yet BMP signaling is reduced, a consequence we attribute to the presence of an ectopic BMP antagonist.

Previous characterizations of SOSTDC1 in the tooth bud confirm a high affinity for multiple BMPs, including BMP2, BMP4, BMP6, and BMP7. When SOSTDC1 was ectopically applied to mouse preosteoblastic MC3T3-E1 cells, it clearly antagonized BMP-mediated osteoblast differentiation (16). Interestingly, our identification of ectopic *Sostdc1* expression in the distal limb and interdigital tissues of *Hoxa13* homozygous mutants (Fig. 4) may also help to explain why *Hoxa13* heterozygous mutant limbs respond more robustly to exogenous BMP2 or BMP7 treatments than their homozygous mutant counterparts (14), since ectopic levels of SOSTDC1 would limit the therapeutic effect afforded by the BMP treatment.

HOX proteins play an essential role in the formation and diversification of serially homologous structures, including insect body segments and flight appendages as well as the vertebrate hindbrain, axial skeleton, and limb (46, 57–63). A mechanism common to the HOX-mediated diversification of these structures is the use of multiple binding sites to modulate target gene expression (59, 63–65). In *Sostdc1*, the removal of the clustered HOXA13 binding sites negated the capacity of HOXA13 to suppress gene expression, a finding consistent with studies in *Drosophila melanogaster*, where multiple Ubx binding sites are required to suppress *spalt* expression in the developing haltere (59). Multiple binding site usage may provide a unique gene-regulatory code to explain how tissues expressing two HOX proteins parse the gene-regulatory signals necessary for tissue development.

Previous reports have identified several genes that are up-regulated by HOXA13 (14, 41); however, in this body of work, we have identified and characterized a gene, *Sostdc1*, that is down-regulated by HOXA13. It is interesting to speculate how HOXA13 may mediate these opposite transcriptional effects through the use of different types of DNA binding sites. Future work to dissect out the roles of different types of HOXA13 binding sites in transcriptional regulation will provide further insight into the function of this transcription factor in embryonic development and disease.

Acknowledgments—We thank Dr. Ed Laufer for providing the phospho-SMAD1/5/8 antibody as well as Diane Sexton and Carley Shaut for expert technical assistance.

REFERENCES

1. Tour, E., Hittinger, C. T., and McGinnis, W. (2005) *Development* **132,** 5271–5281
2. Lei, H., Juan, A. H., Kim, M. S., and Ruddle, F. H. (2006) *Proc. Natl. Acad. Sci. U. S. A.*
3. Wang, N., Kim, H. G., Cotta, C. V., Wan, M., Tang, Y., Klug, C. A., and Cao, X. (2006) *EMBO J.* **25,** 1469–1480
4. Williams, T. M., Williams, M. E., Heaton, J. H., Gelehrter, T. D., and Innis, J. W. (2005) *Nucleic Acids Res.* **33,** 4475–4484
5. Moens, C. B., and Selleri, L. (2006) *Dev. Biol.* **291,** 193–206
6. Salsi, V., and Zappavigna, V. (2006) *J. Biol. Chem.* **281,** 1992–1999
7. Catron, K. M., Iler, N., and Abate, C. (1993) *Mol. Cell. Biol.* **13,** 2354–2365
8. Pellerin, I., Schnabel, C., Catron, K. M., and Abate, C. (1994) *Mol. Cell. Biol.* **14,** 4532–4545
9. Williams, T. M., Williams, M. E., and Innis, J. W. (2005) *Dev. Biol.* **277,** 457–471
10. Treisman, J., Gonczy, P., Vashishtha, M., Harris, E., and Desplan, C. (1989) *Cell* **59,** 553–562
11. Mortlock, D. P., and Innis, J. W. (1997) *Nat. Genet.* **15,** 179–180
12. Fromental-Ramain, C., Warot, X., Messadecq, N., LeMeur, M., Dolle, P., and Chambon, P. (1996) *Development* **122,** 2997–3011
13. Stadler, H. S., Higgins, K. M., and Capecchi, M. R. (2001) *Development* **128,** 4177–4188
14. Knosp, W. M., Scott, V., Bachinger, H. P., and Stadler, H. S. (2004) *Development* **131,** 4581–4592
15. Phelan, M. L., Sadoul, R., and Featherstone, M. S. (1994) *Mol. Cell. Biol.* **14,** 5066–5075
16. Laurikkala, J., Kassai, Y., Pakkasjarvi, L., Thesleff, I., and Itoh, N. (2003) *Dev. Biol.* **264,** 91–105
17. Kassai, Y., Munne, P., Hotta, Y., Penttila, E., Kavanagh, K., Ohbayashi, N., Takada, S., Thesleff, I., Jernvall, J., and Itoh, N. (2005) *Science* **309,** 2067–2070
18. Workman, C. T., Yin, Y., Corcoran, D. L., Ideker, T., Stormo, G. D., and Benos, P. V. (2005) *Nucleic Acids Res.* **33,** W389–392
19. Morgan, E. A., Nguyen, S. B., Scott, V., and Stadler, H. S. (2003) *Development* **130,** 3095–3109
20. Manley, N. R., and Capecchi, M. R. (1995) *Development* **121,** 1989–2003
21. Tuerk, C., and Gold, L. (1990) *Science* **249,** 505–510
22. Liu, J., and Stormo, G. D. (2005) *Nucleic Acids Res.* **33,** e141
23. Maruyama, M., Ichisaka, T., Nakagawa, M., and Yamanaka, S. (2005) *J. Biol. Chem.* **280,** 24371–24379
24. Szymczyna, B. R., and Arrowsmith, C. H. (2000) *J. Biol. Chem.* **275,** 28363–28370
25. Yanagita, M., Oka, M., Watabe, T., Iguchi, H., Niida, A., Takahashi, S., Akiyama, T., Miyazono, K., Yanagisawa, M., and Sakurai, T. (2004) *Biochem. Biophys. Res. Commun.* **316,** 490–500
26. Frazer, K. A., Pachter, L., Poliakov, A., Rubin, E. M., and Dubchak, I. (2004) *Nucleic Acids Res.* **32,** W273–W279
27. Mayor, C., Brudno, M., Schwartz, J. R., Poliakov, A., Rubin, E. M., Frazer, K. A., Pachter, L. S., and Dubchak, I. (2000) *Bioinformatics* **16,** 1046–1047
28. Zwijsen, A., Verschueren, K., and Huylebroeck, D. (2003) *FEBS Lett.* **546,** 133–139
29. Guha, U., Gomes, W. A., Kobayashi, T., Pestell, R. G., and Kessler, J. A.

(2002) *Dev. Biol.* **249,** 108–120
30. Capdevila, J., and Johnson, R. L. (1998) *Dev. Biol.* **197,** 205–217
31. Fitzwater, T., and Polisky, B. (1996) *Methods Enzymol.* **267,** 275–301
32. Benson, G. V., Nguyen, T. H., and Maas, R. L. (1995) *Mol. Cell. Biol.* **15,** 1591–1601
33. Shen, W. F., Montgomery, J. C., Rozenfeld, S., Moskow, J. J., Lawrence, H. J., Buchberg, A. M., and Largman, C. (1997) *Mol. Cell. Biol.* **17,** 6448–6458
34. Jave-Suarez, L. F., Winter, H., Langbein, L., Rogers, M. A., and Schweizer, J. (2002) *J. Biol. Chem.* **277,** 3718–3726
35. Godwin, A. R., Stadler, H. S., Nakamura, K., and Capecchi, M. R. (1998) *Proc. Natl. Acad. Sci. U. S. A.* **95,** 13042–13047
36. Davis, A. P., and Capecchi, M. R. (1996) *Development* **122,** 1175–1185
37. Favier, B., Rijli, F. M., Fromental-Ramain, C., Fraulob, V., Chambon, P., and Dolle, P. (1996) *Development* **122,** 449–460
38. Shanmugam, K., Featherstone, M. S., and Saragovi, H. U. (1997) *J. Biol. Chem.* **272,** 19081–19087
39. Shanmugam, K., Green, N. C., Rambaldi, I., Saragovi, H. U., and Featherstone, M. S. (1999) *Mol. Cell. Biol.* **19,** 7577–7588
40. Shen, W. F., Chang, C. P., Rozenfeld, S., Sauvageau, G., Humphries, R. K., Lu, M., Lawrence, H. J., Cleary, M. L., and Largman, C. (1996) *Nucleic Acids Res.* **24,** 898–906
41. Williams, T. M., Williams, M. E., Kuick, R., Misek, D., McDonagh, K., Hanash, S., and Innis, J. W. (2005) *Dev. Biol.* **279,** 462–480
42. Penkov, D., Tanaka, S., Di Rocco, G., Berthelsen, J., Blasi, F., and Ramirez, F. (2000) *J. Biol. Chem.* **275,** 16681–16689
43. Chang, C. P., Brocchieri, L., Shen, W. F., Largman, C., and Cleary, M. L. (1996) *Mol. Cell. Biol.* **16,** 1734–1745
44. Chang, C. P., Shen, W. F., Rozenfeld, S., Lawrence, H. J., Largman, C., and Cleary, M. L. (1995) *Genes Dev.* **9,** 663–674
45. Mann, R. S., and Affolter, M. (1998) *Curr. Opin. Genet. Dev.* **8,** 423–429
46. Warren, R. W., Nagy, L., Selegue, J., Gates, J., and Carroll, S. (1994) *Nature* **372,** 458–461
47. Huang, H., Rastegar, M., Bodner, C., Goh, S. L., Rambaldi, I., and Featherstone, M. (2005) *J. Biol. Chem.* **280,** 10119–10127
48. Zhao, Y., and Potter, S. S. (2001) *Development* **128,** 3197–3207
49. Burke, A. C., and Feduccia, A. (1997) *Science* **278,** 666–668
50. Hinchliffe, J. R. (2002) *Int. J. Dev. Biol.* **46,** 835–845
51. Capdevila, J., and Izpisua Belmonte, J. C. (2001) *Annu. Rev. Cell Dev. Biol.* **17,** 87–132
52. Yoon, B. S., Ovchinnikov, D. A., Yoshii, I., Mishina, Y., Behringer, R. R., and Lyons, K. M. (2005) *Proc. Natl. Acad. Sci. U. S. A.* **102,** 5062–5067
53. Kobayashi, T., Lyons, K. M., McMahon, A. P., and Kronenberg, H. M. (2005) *Proc. Natl. Acad. Sci. U. S. A.* **102,** 18023–18027
54. Healy, C., Uwanogho, D., and Sharpe, P. T. (1996) *Ann. N. Y. Acad. Sci.* **785,** 261–262
55. Healy, C., Uwanogho, D., and Sharpe, P. T. (1999) *Dev. Dyn.* **215,** 69–78
56. Brunet, L. J., McMahon, J. A., McMahon, A. P., and Harland, R. M. (1998) *Science* **280,** 1455–1457
57. Burke, A. C., Nelson, C. E., Morgan, B. A., and Tabin, C. (1995) *Development* **121,** 333–346
58. Cohn, M. J., and Tickle, C. (1999) *Nature* **399,** 474–479
59. Galant, R., Walsh, C. M., and Carroll, S. B. (2002) *Development* **129,** 3115–3126
60. Lewis, E. B. (1978) *Nature* **276,** 565–570
61. Mohit, P., Makhijani, K., Madhavi, M. B., Bharathi, V., Lal, A., Sirdesai, G., Reddy, V. R., Ramesh, P., Kannan, R., Dhawan, J., and Shashidhara, L. S. (2006) *Dev. Biol.* **291,** 356–367
62. Ruvinsky, I., and Gibson-Brown, J. J. (2000) *Development* **127,** 5233–5244
63. Weatherbee, S. D., Halder, G., Kim, J., Hudson, A., and Carroll, S. (1998) *Genes Dev.* **12,** 1474–1482
64. Capovilla, M., Kambris, Z., and Botas, J. (2001) *Development* **128,** 1221–1230
65. Capovilla, M., Brandt, M., and Botas, J. (1994) *Cell* **76,** 461–475